Chapter 7
Monitoring Population Membrane Potential Signals from Neocortex

Jianmin Liang, Weifeng Xu, Xinling Geng, and Jian-young Wu

Abstract Voltage-sensitive dyes (VSDs) and optical imaging are useful tools for studying spatiotemporal patterns of population neuronal activity in cortex. Because fast VSDs respond to membrane potential changes with microsecond temporal resolution, these are better suited than calcium indicators for recording rapid neural signals. Here we describe methods for using a 464 element photodiode array and fast VSDs to record signals ranging from large scale network activity in brain slices and in vivo mammalian preparations with sensitivity comparable to local field potential (LFP) recordings. With careful control of dye bleaching and phototoxicity, long recording times can be achieved. Absorption dyes have less photo-toxicity than fluorescent dyes. In brain slices, the total recording time in each slice can be 1,000–2,000 s, which can be divided into hundreds of short recording trials over several hours. In intact brains when fluorescent dyes are used, reduced light intensity can also increase recording time. In this chapter, we will discuss technical details for the methods to achieve reliable VSD imaging with high sensitivity and long recording time.

Keywords Voltage-sensitive dyes • NK3630 • RH486 • RH1691 • Brain slice • Visual cortex • Propagating waves • Spirals • Coupled oscillators

J. Liang
Department of Neuroscience, Georgetown University Medical Center, 207A, Basic Science Building, 3900 Reservoir Road NW, Washington, DC 20057, USA

Department of Pediatrics, First Bethune Hospital of Jilin University, Changchun 130021, P. R. China

W. Xu • J.-y. Wu (✉)
Department of Neuroscience, Georgetown University Medical Center, 207A, Basic Science Building, 3900 Reservoir Road NW, Washington, DC 20057, USA
e-mail: wuj@georgetown.edu

X. Geng
Department of Neuroscience, Georgetown University Medical Center, 207A, Basic Science Building, 3900 Reservoir Road NW, Washington, DC 20057, USA

Shoool of Biomedical Engineering, Capital Medical University, Beijing 100069, P. R. China

1   Introduction

Voltage-sensitive dye (VSD) imaging, an optical method of measuring transmembrane potential, has been undergoing constant development since pioneering work published about 40 years ago (Cohen et al. 1968; Tasaki et al. 1968; Chap. 1). With the development of better dyes and specialized apparatus, the method has gradually evolved from a technological demonstration of feasibility into a powerful experimental tool for imaging the activity of excitable tissues. After a heroic screening effort during which thousands of dye compounds were tested for voltage sensitivity (Gupta et al. 1981; Grinvald et al. 1982a, 1982b; Loew et al. 1992; Shoham et al. 1999), dozens of dyes were found useful, and many analogs became commercially available. These dyes all have very fast response times (<1 µs) and excellent linearity over the entire physiological range (Ross et al. 1977), but all show only small fractional changes in absorption or fluorescence. In biological tissues, these fractional changes amount to only about 10^{-2} to 10^{-5} of the resting light intensity per 100 mV of membrane potential change.

Until more sensitive probes become available, measurements of fast voltage activity are carried out using traditional organic dyes characterized by relatively low sensitivity in terms of fractional change in light intensity per unit change in membrane potential ($\Delta I/I$). However, a small fractional change in light intensity does not necessarily equate to poor signal-to-noise ratio. In this chapter, we will discuss methods to achieve high signal-to-noise ratio recordings of VSD activity in brain slices and in intact rodent cortex. If vibration noise is properly reduced, a signal-to-noise ratio of 5–30 can be achieved in single recording trials. This signal-to-noise ratio is sufficient to examine the initiation and propagation of wave activity in the cortical local circuits. Also, this high sensitivity is critical for examining the dynamics of population neuronal activities and activity patterns, such as spiral waves, with spatiotemporal structures that are too complex to be analyzed by averaging. Under *in vivo* conditions, new blue dyes (see Chap. 2) reduce the pulsation noise and allow us to achieve high sensitivity in single trials.

2   Cortical Slice, Solutions and Recording Conditions

The preparation of slices for imaging neuronal population activity is different from that for cellular electrophysiology. For imaging of population events, local circuits need to be well preserved with a larger proportion of viable neurons and functioning synapses. Thinner slices usually have poor signal-to-noise ratio, probably because of more extensive cell damage and poor cell recovery. We prefer slices with thickness of 400–600 µm, because local circuits can be better preserved. Thicker slices need to be well perfused from both sides with a fast perfusion rate.

In brief, following NIH animal care and use guidelines and institutional animal care committee protocols, the animals are deeply anesthetized with halothane and

quickly decapitated (using a Stoelting small animal decapitator). The whole brain is carefully harvested and chilled for 90 s in cold (0–4 °C) artificial cerebrospinal fluid (ACSF) for slicing containing (in mM) 250 sucrose, 3 KCl, 2 $CaCl_2$, 2 $MgSO_4$, 1.25 NaH_2PO_4, 27 $NaHCO_3$, 10 dextrose, and saturated with 95 % O_2, 5 % CO_2. Then the brain is blocked and sliced at 400–600 μm thickness on a vibratome stage (e.g., 752 M Vibroslice, Campden Instruments, Sarasota, FL).

Brain slices can be cut in several directions to conserve different aspects of cortical circuitry. For example, coronal sections can preserve the cortical columns such as whisker barrels. Oblique directions can preserve the thalamocortical connections (Agmon and Connors 1992; MacLean et al. 2006). Slices cut tangentially can best preserve the horizontal connections in layer II–III to observe 2D waves such as spirals (Huang et al. 2004).

After slicing, the slices are transferred into a holding chamber with holding ACSF, containing (in mM): 126 NaCl, 2.5 KCl, 2 $CaCl_2$, 2 $MgSO_4$, 1.25 NaH_2PO_4, 26 $NaHCO_3$, 10 dextrose. We use a large holding chamber, containing about 500 ml of holding ACSF, which can keep slices viable for 8–12 h. The holding solution is bubbled with a mixture of 95 % O_2 and 5 % CO_2, and is slowly circulated by a magnetic stirring bar. Stirring provides a slow but steady convection around the slice for delivering oxygen and washing out noxious molecules produced by the cold shock and the trauma of slicing. Slices must be incubated for at least 2 h before the experiments to allow for recovery from the acute trauma.

3   Staining Slice with Voltage-Sensitive Dye

Slices are stained with the VSD before imaging experiment. We prefer lower dye concentrations and longer staining times of 1–2 h instead of shorter staining time under higher dye concentrations. Longer staining time allows the cells deep in the tissue to be evenly stained. Since staining time is long, aeration and convection are critical. The staining chamber contained about 50 ml of holding ACSF, bubbled slowly with a mixture of 95 % O_2 and 5 % CO_2 (about 1 bubble/s) and circulated by a stirring bar. Dyes have a tendency to be concentrated on the air-water interface and slower bubbling with large bubbles can reduce the depletion of the dye from the solution. For absorption measurements, we use 5–20 μg/ml of an oxonol dye, NK3630 (first synthesized by R. Hildesheim and A. Grinvald as RH482; available from Nippon Kankoh-Shikiso Kenkyusho Co.,Ltd., Japan, Charkit chemical Corp, Darien, CT). For fluorescence measurements, we use 10–50 μg/ml of fluorescent dye, RH414 or RH795 (first synthesized by R. Hildesheim and A. Grinvald; available from Molecular Probes/Invitrogen). After staining, the slices are transferred back to the holding chamber to rinse out excess dye and for incubation until recording.

4 Imaging Chamber for Brain Slice

During VSD imaging, the slice is mounted in a perfusion chamber on a microscope stage. The slice is set on a mesh in the center of the chamber so that both sides of the slice are well perfused. The perfusion speed is 6–10 ml per minute (80 drops/min). Perfusing ACSF contains (in mM) 126 NaCl, 2.5 KCl, 2 $CaCl_2$, 1.5 $MgSO_4$, 1.25 NaH_2PO_4, 26 $NaHCO_3$, and 10 dextrose. The solution is warmed prior to perfusion with fine Tygon tubing wound on a temperature-controlled heating block. The tubing in the heating block is about 100 cm long and the solution is heated from room temperature to 28–32 °C when entering the perfusion chamber.

5 Imaging Rat Cortex In Vivo

For rodent cortex in vivo we use the 'blue' dyes, RH1691 or RH1938, developed by Amiram Grinvald's group (Shoham et al. 1999), The blue dyes are excited by yellow light (630 nm), which does not overlap with the wavelengths absorbed by hemoglobin (510–590 nm). This virtually eliminates heart beat pulsation artifacts. By comparison, the traditional 'red' dyes, such as RH795 or Di-4-ANEPPS have pulsation artifacts that can sometimes exceed the evoked cortical signals by an order of magnitude (Orbach et al. 1985; London et al. 1989; Shoham et al. 1999; Grinvald and Hildesheim 2004; Ma et al. 2004).

Staining mammalian cortex in vivo requires great care with regard to the exposed cortex and the animal's physiological condition. An irritated cortex often leads to poor staining. Briefly, animals are pretreated with atropine sulfate (40 µg/kg IP) approximately 30 min prior to anesthetic induction. The animals are anesthetized with 1.5–2 % isoflurane in air via trachea catheter (16 G over-the-needle) and ventilated by a small animal respirator (Harvard Apparatus) at a rate of 60–100/min and volume of 2–4 ml. Rate and volume are adjusted to maintain an inspiratory pressure of ~5 cm H_2O and an end-tidal carbon dioxide value of 26–28 mmHg. A cranial window (~5 mm in diameter) is drilled and bone is carefully separated from the dura, which is left intact. Leaving the dura intact significantly reduces movement artifacts during optical recording (London et al. 1989; Lippert et al. 2007). Nontraumatic craniotomy is important for optimal staining. Irritated brain can appear reddish (due to increased blood flow), or CSF pressure can increase the potential subdural space, which leads to poor staining. Dexamethasone sulfate (1 mg/kg IP) can be given 24 h prior to the experiment, to reduce the inflammatory response of the dura. Voltage-sensitive dye RH 1691 (Optical Imaging) is dissolved at 2 mg/ml in artificial CSF solution, and staining is done through the intact dura mater. Drying dura before staining can increase the dural permeability to the dye. A temporary staining chamber is constructed around the craniotomy with silicone valve grease. Approximately 200 µl of dye solution will stain an area of 5 mm in diameter. During staining, the dye solution is continuously

circulated by a custom-made perfusion pump (London et al. 1989). The pump has gear motor which gently presses the rubber nipple of a Pasteur pipette once every few seconds. The tip of this pipette is placed in the staining solution and performs a gentle, back-and-forth circulation of a small amount of dye (~100 µl). Staining lasts for 90 min, followed by washing with dye-free ACSF for >15 min. For further discussion of staining cortex in vivo see Lippert et al. 2007.

6   Imaging Device

A 469-element photodiode array (WuTech Instruments, Gaithersburg, MD) is used for VSD imaging (Fig. 7.1a). This array consists of 464 individual photodiodes, each glued to an end of an optical fiber (750 µm in diameter). All the optical fibers are bundled coherently into a hexagonal aperture (19 mm in diameter). With the hexagonal bundling and coupling of the optical fibers, the dead space on the imaging aperture is reduced (8 % of active/inactive space). The array can be mounted on standard camera port of a microscope (such as a "C" mount).

Photo-current from each diode is fed into a two stage amplifier circuit (Fig. 7.1b). The first stage converts the photocurrent into voltage-signal, about 5 V in our absorption measurements. This voltage signal has two components: one is a large DC voltage corresponding to resting light intensity. The second component is the dye signal, a small fractional change in the resting light. This signal ranges from 10^{-5} to 10^{-3} for absorption measurements and 10^{-3} to 10^{-2} for fluorescent measurements. For absorption measurements, the output of the first stage amplifier has a very small signal of 0.05–5 mV riding on top of a large 5 V resting light signal. If, for example, this 5 V + 0.5 mV is digitized directly by a 14 bit A/D converter, the 0.5 mV signal would be digitized by less than 1 bit, which is not sufficiently precise. In order to digitize 0.5 mV signal with at least 7 bit range, a DC subtraction circuit is used between the first and second stage amplifiers, for a hardware background subtraction (Fig. 7.1b).

The DC subtraction is done at the beginning of each recording trial when the illumination light is turned on. At this time the "reset" switch is closed and the capacitor C is charged to the output voltage of the resting light intensity. After about 80 ms when the C is fully charged, the reset switch is opened to allow recording to begin. Since the capacitor is charged to the same voltage as the resting light intensity at the input of the second stage, the voltage from the first stage and the voltage on the capacitor will be equal and have opposite polarities, resulting in a subtracted zero resting light intensity voltage. The second stage can then apply $100\times$ to $1,000\times$ voltage gain to the signal. As a result, a $100\times$ voltage gain will extend the dynamic range of the imaging device by ~8 bit. Since resting light intensity on different detectors can differ largely, each diode needs a dedicated DC subtraction circuit between the first and second amplifier stage (Cohen and Lesher 1986; Wu and Cohen 1993). For this reason, the photodiode array with high spatial resolution is bulky and difficult to manufacture.
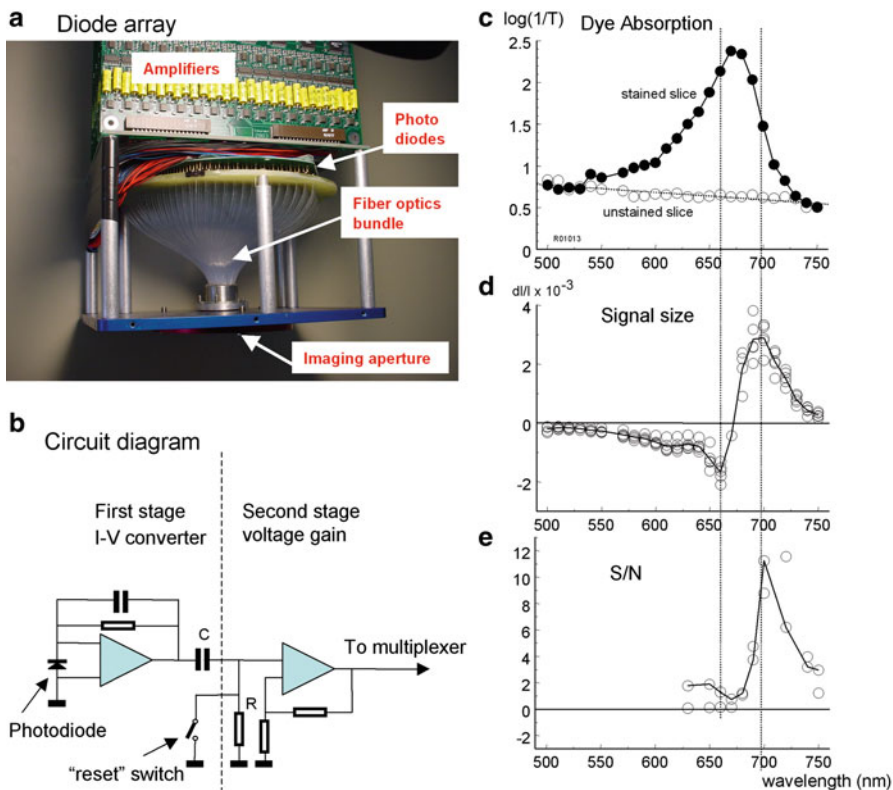
Fig. 7.1 Photodiode array, absorption spectra and signal-to-noise ratio. (**a**) WuTech 469 V photodiode array, a commercial version of the photodiode arrays developed by Cohen group (Cohen and Lesher 1986). WuTech 469 V has an integrated design with all 464 diode amplifiers housed together with the fiber optic bundles. This reduces both light and electrical interference. The hexagonal optic fiber bundle contains 469 optical fibers. Each of fibers is glued to a PIN photodiode and each diode is wired to a dedicated two-stage amplifier (**b**) Circuit diagram of one amplifier channel. The first stage converts the photocurrent outflow of the diode into voltage; the reset switch and the coupling capacitor C subtract the DC component in the light. The second stage provides a 100× voltage gain to boost the effective dynamic range. (**c**) The absorption spectrum of unstained slices (*unfilled circles*) and a slice stained with NK3630 (*solid dots*). (**d**) VSD signal amplitude at different wavelengths. Note that the maximum amplitude is not at the peak absorbance. (**e**) Signal-to-noise ratio at different wavelengths. (Modified from Jin et al. 2002)

We use a 14 bit data acquisition board (Microstar Laboratories, Bellevue, WA) installed in a desktop PC computer. The second stage amplifier also contains a low pass filter with 333 Hz corner frequency; this hardware filter will further improve the quality of the analog signal before digitizing. The sampling speed needs to be faster than any events to be measured, usually 1,000–2,000 frames/s are adequate for imaging brain slices.

7 Microscope and Light Source

For imaging with absorption dyes, inexpensive low NA objectives and a conventional 100 W tungsten halogen lamp from an ordinary research microscope can provide excellent results. 735 nm LED illuminator (ThorLabs) can also be used for illumination. LED illuminator runs cool, which appears to be better than the hot halogen lamp. However, LED can flicker at much higher frequency and so it is much more difficult to reduce the light fluctuation down to 10^{-5} of the illumination intensity (ordinary "super stable" LED driver uses switching circuit and only provides noise level down to 10^{-3}). Battery and a constant current source with linear (non-switching) circuits may be necessary for powering the LED.

For large imaging field such as that shown in Figs. 7.5, 7.6, and 7.7, we use a 5× 0.12 NA objective (Zeiss). When working with smaller imaging fields, 20× (0.6 NA, water immersion, Zeiss) or 40× (0.75 NA, water immersion, Zeiss) can be used accordingly. When a 5× objective is used, each photodetector of a 464-diode array receives light from a tissue area of 150 μm in diameter.

In absorption measurements in brain slice, the resting light intensity is usually about one billion photons per millisecond on each optical detector. The dye molecules absorb most of the light in the wavelength used for the measurement. Unstained tissue slices absorb an insignificant fraction of the light (Fig. 7.1c). The resting light intensity on each photodiode is about 10^9 photons per milliseconds.

For in vivo imaging of mammalian cortex with fluorescent dyes, high light gathering optics are necessary. We use a 5× "macroscope", which provides an imaging field of 4 mm in diameter (Kleinfeld and Delaney 1996; Prechtl, Cohen et al. 1997). The macroscope uses a commercial video camera lens (Navitar, 25 mm F0.95). This inexpensive camera lens provides a high numerical aperture of 0.45, compared to an ordinary 4× microscope objective (~0.12 NA). Such a high numerical aperture can gather about 100 times more light, significantly increasing the signal-to-noise ratio for in vivo fluorescent imaging. A tungsten halogen filament lamp (12 V, 100 W, Zeiss) or 630 nm LED (ThorLabs) can be used for illumination. Again the LED may need to be powered by a battery and a linear constant current source.

8 Optical Filters

Figure 7.1c shows the absorption spectrum of a cortical slice stained with dye NK3630 and an unstained slice. The unstained slice has a relatively even transmission with a tendency to absorb less at longer wavelengths (Fig. 7.1c, open circles). The stained slice has a peak of absorption around 670 nm (Fig. 7.1c, solid circles) and the peak stays the same after a long wash with dye-free ACSF. The light transmission at 670 nm (peak absorption) through a 400 μm well stained slice is reduced to 1/10–1/50 of that of unstained slices.

In Fig. 7.1d, e, the amplitudes of the dye signal (dI/I) and signal-to-noise ratio are plotted against wavelength. The dI/I and signal-to-noise ratio reaches a maximum at 705 nm. The signal decreases significantly at wavelengths shorter than 690 nm and reaches a minimum at ~675 nm. At wavelengths shorter than 670 nm the signal became larger but the polarity of the signal reverses. The signal reaches a second maximum at 660 nm. After the 660 nm peak, the signal decreases gradually and becomes undetectable at wavelengths of 550 nm or shorter. The signal-to-noise ratio at the 660 nm was not large in our actual measurement (Fig. 7.1e), probably due to less resting light at the wavelength. The plots in Fig. 7.1c–e indicate several useful wavelengths: for non-ratiometric measurement, band pass filtering around 705 nm should yield the largest signal; an alternating illumination at 700 and 660 nm may be used for ratiometric measurements; illumination at 675 nm should provide a minimum VSD signal, which can be used for measuring light scattering or for distinguishing VSD from broad-band intrinsic signals.

Optical filters for NK3630 should have a center wavelength around 705 nm. The bandwidth of the filter depends upon several factors: When the signal is small and shot noise is a limiting factor, a wider bandpass allows more light and thus increases the signal-to-noise ratio. In this case, the filter should have a center wavelength of 715 nm and a bandwidth of ± 30 nm. When measuring large signals and when a long total recording time is needed, a narrow band filter of 705 ± 15 nm should be used to reduce the illumination intensity. When the illumination light is strong enough, using narrow band filters helps to get larger signals and reduce dye bleaching and phototoxicity. Since the measurement wavelength is between 700 and 750 nm (Fig. 7.1d, e), the heat filter (infrared filter) in front of the light housing absorbs most energy in this range. For absorption measurements, this heat filter must be removed from the light path.

When the 735 nm LED illuminator is used for NK3630, the excitation filter may be omitted. This increases the light throughput significantly. However, the LED provides high intensity from 735 to 755 nm, which gives little VSD signal but large intrinsic optical signals (light scattering). The intrinsic optical signal appears as a large and slow drift of the baseline of the VSD recording traces (Fig. 7.3b-2, trace 2). In some recordings a flat baseline is preferred and a narrow band filter of 735 ± 10 nm can be used to reduce intrinsic signal.

For imaging mammalian cortex with the blue dyes, a filter cube (from Chroma or Semrock) is used, with a 630 ± 15 nm excitation filter, 655 nm dichroic mirror (Chroma Technology) and a 695 nm long pass filter. This filter cube fits well for both halogen lamp and LED. Köhler illumination is achieved with the macroscope.

9   Detecting Vibration Noise

Vibration noise is often the dominant noise source when recording absorption signals from brain slices. Vibration causes a movement of the image related to a photodetector and thus causes a fluctuation of the light intensity. Absorption

measurement is characterized by small fractional changes and a high resting light intensity, so it is more sensitive to movement of the preparation compared to fluorescence measurements.

Vibration noise is proportional to the resting light intensity while shot noise is proportional to the square root of the light intensity. Thus when illumination intensity increases, vibration noise will ultimately become dominant. Above the level where vibration noise equals the shot noise, signal-to-noise ratio will no longer increase with higher illumination intensity. Therefore vibration control in many situations determines the ultimate signal-to-noise ratio.

In practice, we use the following method to evaluate the vibration noise on any given experimental set-up. (1) Under Koehler illumination, reduce the field diaphragm of the microscope so that a clear image of the diaphragm (as a round hole with a sharp edge) is formed in the field of view and projects the image onto the diode array. The sharp edge of the image generates a near maximum contrast on the imaging system. Due to vibration, the edge may move in the image plane so that the light intensity on some detectors recording the diaphragm edge will fluctuate between minimum and maximum. The intensity change on these photodetectors will reflect the worst possible scenario of vibration noise. The power spectrum of the signals from these noisy detectors viewing the edge of the field diaphragm can help to determine the vibration source. In many modern buildings, ~30 Hz floor vibrations are caused by ventilation fan motors attached to the building structure. Vibrations at less than 5 Hz sometimes come from movement of the building in wind, or resonance of the floor. When the experimental stage is properly isolated, noise at the edge of the field diaphragm should be no larger than that in the center of the aperture, indicating that the dominant noise is no longer vibration, but shot noise. With the chamber and preparation inserted into the light path, the vibration noise may also become larger because of the vibration of the water-air interface. A cover slip or water immersion lens can eliminate this vibration noise.

We find that many air tables and active isolation platforms perform poorly in filtering vibrations below 5 Hz. A novel isolation stage designed for atomic force microscopy, the "Minus K" table (www.minusk.com), is approximately ten times better at attenuating these frequencies than some standard air tables. With the Minus K table, the vibration noise can be reduced to below the level of shot noise at a resting light intensity of $\sim 10^{11}$ photons/ms/mm^2.

10   Data Acquisition and Analysis

NeuroPlex, developed by A. Cohen and C. Bleau of RedShirtImaging, LLC, Decatur, GA, is a versatile program for acquiring and analyzing VSD data. The program can display the data in the form of traces for numerical analysis and pseudo color images for studying the spatiotemporal patterns. Data analysis can also be done with scripts written in MatLab (Mathworks). The singular value

decomposition (SVD) method (Precthl et al. 1997) is a very effective way for removing random noise (e.g., shot noise) from the signal.

The figures in this chapter are examples of data display where the signal from the local field potential (LFP) electrode and that of an optical detector viewing the same location are plotted together. The spatiotemporal patterns of the activity are often presented with pseudo color maps (Senseman et al. 1990). To compose a pseudo color map, the signal from each individual detector is normalized to its own maximum amplitude (peak = 1 and baseline/negative peak = 0), and a scale of 16 or 256 colors is linearly assigned to the values between 0 and 1.

The imaging data are acquired at a high rate, usually at approximately 1,600 frames per second. Figures in published papers usually include only a few frames selected from this large imaging series. The signal-to-noise ratio is usually defined as the amplitude of the VSD signal divided by the root mean square (RMS) value of the baseline noise. Since most population neuronal activity in the neocortex is below 100 Hz, a low pass filter can be used to reduce RMS noise and improve the signal-to-noise ratio.

11   Sensitivity

The sensitivity of VSD measurement can be estimated by comparing the measurement with LFP recorded from the same tissue. Achieving a high sensitivity comparable to LFP recordings is important not only for detecting small population activity, but also for detecting spatiotemporal patterns when multiple trial averaging is not allowed.

In the experiment shown in Fig. 7.2, we used a rat neocortical slice stained with NK3630. Cortical layers II–III were monitored optically and a LFP electrode was placed inside of the imaging field of the array (Fig. 7.2a). Electrical stimulation is delivered in deep cortical layers and the evoked neuronal response in layers II–III is monitored both optically by the diode array and electrically by the local field potential electrode (Fig. 7.2b). At low stimulus intensities (0.8–2 V, 0.04 ms), the amplitude of the VSD and LFP is approximately linear with the stimulus intensity (Fig. 7.2d). Although the thresholds for VSD and LFP measurements varied in different slices, we found that the sensitivity of the VSD measurement is always higher than that of the LFP if the slice was properly stained (Jin et al. 2002).

In an ideal situation, the sensitivity of the measurement is limited only by the shot noise (the statistical fluctuations in the photon flux). In measurements using absorption dyes, the shot noise can be dominant when the resting light intensity is higher than 5×10^9 photons/ms/mm^2. This resting light intensity can be achieved with an ordinary 100 W tungsten-halogen filament lamp. Since the amplitude of the VSD signal is proportional to the resting light intensity while the shot noise is proportional to the square root of the resting light intensity, the signal-to-noise ratio is proportional to the square root of the resting light intensity (Cohen and Lesher 1986). Therefore increasing the illumination light can increase the signal-to-noise
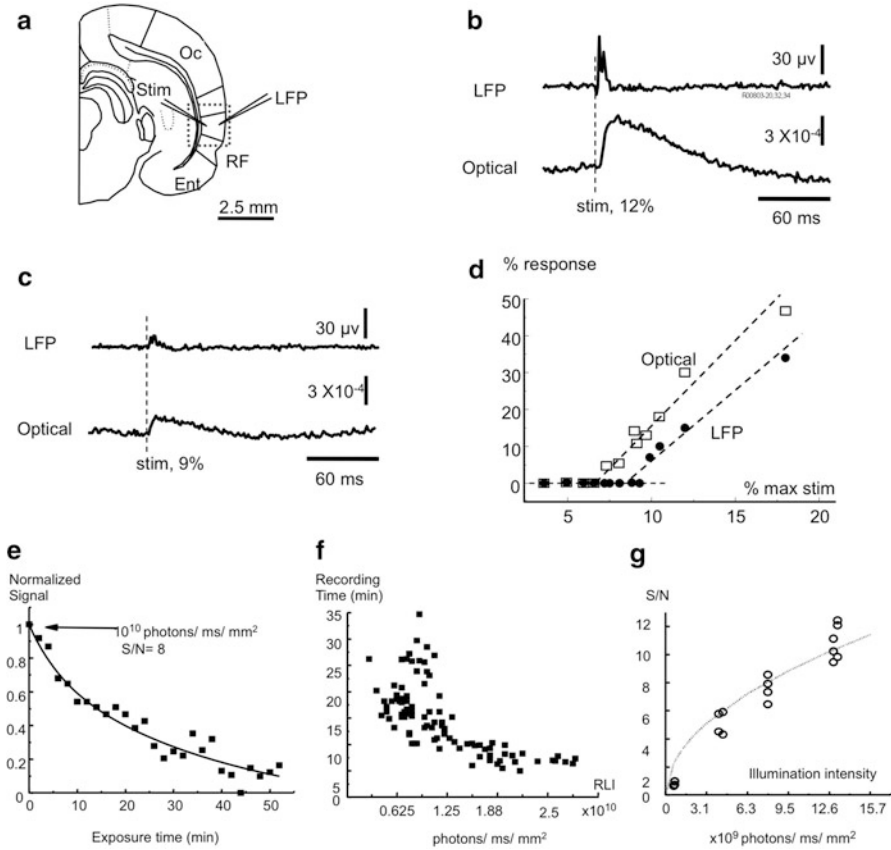
Fig. 7.2 Sensitivity of VSD imaging, dye bleaching and total recording time. (**a**) Experimental arrangement. Rat cortical slices are stained with NK3630 and imaged with a 5× 0.12 NA objective. The *broken line* marks the imaging field. Local field potential (LFP) is recorded from layer II–III, where a photo detector is viewing an area of 200×200 μm^2 of the tissue recorded by the electrode. Electrical stimulation (Stim) is delivered to deep layers. (**b**) At 12 % of the stimulation intensity that generated a maximal response, neuronal response is visible in both LFP and VSD signals. Note that stimulation artifact does not appear in the VSD signal. (**c**) A smaller stimulus evokes a reduced response in both VSD and LFP signals. A series of stimuli around the response threshold were applied to test the sensitivity of VSD recordings. (**d**) A plot of response amplitude at different stimulation intensities. Note that both VSD signals (*squares*) and LFP signals (*dots*) are linearly related to the stimulation intensity, and the sensitivity of VSD appears higher than that of the LFP. (**e**) Reduction of VSD signals due to light exposure. The slice was stained with NK3630 and exposed to an illumination intensity of 5×10^{11} photons/ms/mm^2 (resting light intensity was ~10^{10} photons/ms/mm^2). The exposures were 2 min trials with 2 min intermittent dark periods. (**f**) The total recording time is defined as the exposure time needed for the VSD signals to decrease to 50 % of the pre-exposure amplitude. The plot was composed of data from ~25 locations in four slices. (**g**) Signal-to-noise ratio of absorption measurement at different resting light intensities. The signal is the neuronal response in cortical layer II–III evoked by an electrical stimulation in deep layers. (Modified from Jin et al. 2002)

ratio. The diode array is a noise free imaging device in a wide range of light intensities when the shot noise dominates, because the dark noise of the system becomes negligible. However, the resting light intensity cannot be increased infinitely. Due to dye bleaching and phototoxicity, resting light intensity is a limiting factor for total recording time from a given field of view (see below).

12 Phototoxicity, Bleaching and Total Recording Time

When stained slices are continuously exposed to high intensity light (e.g., ~10^{12} photons/ms/mm^2), noticeable decline of both LFP and VSD signals is observed after 5–10 min. We refer to this reduction in electrical activity caused by light exposure as phototoxicity or photodynamic damage (Cohen and Salzberg 1978). Phototoxicity in cortical slices appears to be irreversible even after a long dark recovery period. Absorption dyes have much less phototoxicity than the fluorescent dye RH795 in brain slice experiments, probably because the latter produces free radicals when it is in the excited state.

Intermittent light exposure significantly reduces phototoxicity. With the same high intensity of 10^{12} photons/ms/mm^2, when the exposure was broken into 2 min sessions with 2 min dark intervals, the phototoxicity of NK3630 was smaller. The LFP signals decreased <30 % after 60 min of total exposure time. The optical signals, however, decreased ~90 % (Fig. 7.2e). We refer to the reduction in optical signal while LFP signals remain unchanged as "bleaching". After long light exposure, bleaching is visible even by eye, as loss of color in the exposed area. Optical signals can not be recovered in the bleached area even if the preparation is re-stained.

We define the total recording time as the exposure time needed to reduce the amplitude of the optical signal to 50 % of the pre-exposure level. Figure 7.2f shows the total recording time at different resting light intensities. Figure 7.2g shows the signal-to-noise ratio at four resting light intensities. Combining the results in Fig. 7.2f, g, we conclude that when illumination intensity is adjusted for a signal-to-noise ratio of 8–10, the total recording time is about 15–30 min. This time can be divided into hundreds of intermittent recording sessions (e.g., 100 of 8 s trials), enough for most of applications.

The total recording time of the fluorescent dye RH795 seems to be limited by phototoxicity. When slices stained with RH795 were illuminated with 520 nm light at an intensity of ~10^{12} photons/ms/mm^2, both LFP and optical signals disappeared in a few trials of 2 min exposures. After the signals disappeared, the fluorescence of the stained tissue remained at ~80 % of the pre-exposure level, suggesting that phototoxicity occurred and bleaching was insignificant.

13 Waveforms of the Population VSD Signal

When a single neuron was simultaneously monitored by a photo detector and an intracellular electrode, the waveforms of the two recordings were remarkably similar (Fig. 7.3a; Ross et al. 1977; Zecevic 1996). However, for population activity, the VSD signal may be greatly different from that recorded with an electrode.

Figure 7.3b compares the waveforms of LFP (top traces) and VSD (bottom traces) recordings during different types of neuronal activity in neocortex. Figure 7.3b-1 shows a short latency ("Fast") response to an electrical stimulus to the white matter. This response has a short latency and the amplitude of VSD signal is proportional to the stimulus intensity. Presumably the response is mainly based on depolarization of neurons stimulated either directly or via a few synapses. The LFP response had a short duration (<30 ms) but the VSD signal from the tissue surrounding the electrode had a much longer duration. This long-lasting optical signal did not appear at 520 nm, indicating that it was a wavelength dependent VSD signal, and not a wavelength-independent light-scattering ("intrinsic") signal. Dye molecules bound to the glial cells may also contribute to this long response due to glial membrane potential change caused by glutamate transporters (Kojima et al. 1999; Momose-Sato et al. 1999).

Figure 7.3b-2 shows the signals from an interictal-like spike (slice bathed in 10 μM bicuculline) evoked by weak electrical shock to the white matter, measured in cortical layers II–III. Interictal-like spikes are all-or-none population events; the amplitude of the dye signal is relatively large and independent of the stimulus intensity. Again, VSD signals had a long duration with a smooth waveform while LFP signals had a short duration and large fluctuations. The VSD signal during an interictal-like spike had an obvious undershoot (downward phase below the baseline following the positive peak). Part of this undershoot also occurred at 520 nm (Fig. 7.3b-2, trace 2), suggesting that it was caused by a light scattering signal. The sign of the light scattering signal under trans-illumination was opposite to that of the VSD signal of NK3630 at 705 nm.

Figure 7.3b-3 shows 40–80 Hz oscillations evoked by an electrical stimulus (Luhmann and Prince 1990; Metherate and Cruikshank 1999). The oscillations are only seen in LFP recordings but not in the VSD signals, suggesting that the local oscillatory populations are small and neurons with different phases are mixed (Wu et al. 2001). The VSD signal amplitude is only about 1/10–1/4 of that of the interictal-like spikes (Fig. 7.3b-2). This indicates that this type of ensemble activity involves a much smaller fraction of active neurons than do interictal-like spikes.

In Fig. 7.3b-4, the waveforms of VSD signals during the three types of population events depicted in Fig. 7.3b-1–b-3 are superimposed, illustrating differences in amplitude and time course. If the neurons are evenly stained, the amplitude of the VSD signal and the amount of synchrony in neuronal activity should have a liner relationship. The same should hold for the relationship between the area under the waveform envelope and the overall depolarization and spikes during the event. Figure 7.3b-4 suggests that the synchrony and duration during different cortical
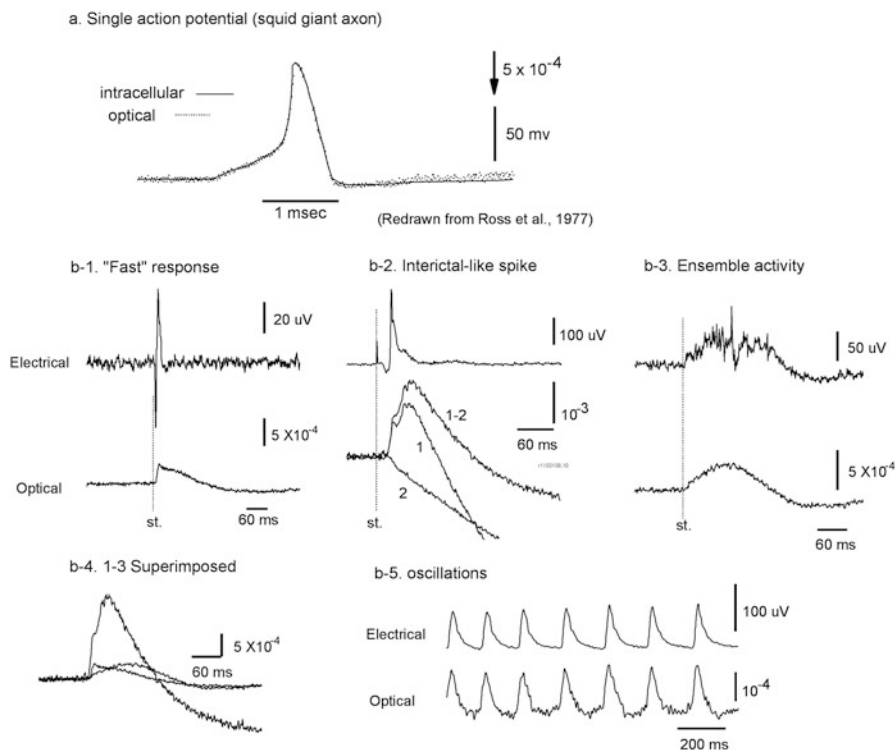
Fig. 7.3 Waveform of optical and electrical recordings. (**a**) VSD and intracellular recordings from a squid giant axon. The axon was stained with absorption dye XVII and the optical signal was measured at 705 nm (*dotted trace*). The actual membrane potential change (*smooth trace*) was simultaneously recorded by an intracellular electrode. The time course of the VSD signal mirrored precisely the time course of membrane potential change. (Redrawn from Ross et al. 1977, with permission from Springer). (**b**) LFP recordings (*top traces*) and VSD recordings (*bottom traces*) during different types of population activity. The recordings were simultaneously made from the same location in cortical layers II–III of rat somatosensory cortical slices. (**b-1**) A short latency activity (fast response) was evoked by an electrical shock to the white matter; the slice was bathed in normal ACSF. (**b-2**) An evoked interictal spike (Tsau et al. 1999); the slice was bathed in 10 μM bicuculline. During this activity, a large fraction of neurons were activated and changes in light scattering also contributed to the signal. Here, trace 1 is the light intensity change at 705 nm; trace 2 is the intensity change at 520 nm, presumably the light scattering signal; subtraction of the signal at the two wavelengths (trace 1–2) estimates the VSD signal without contamination from light scattering signal. (**b-3**) An evoked population oscillation (Wu et al. 2001). (**b-4**) VSD traces of **b-1**, **b-2** (trace 1–2), and **b-3** are superimposed, showing the difference in amplitude and time course. (**b-5**) A spontaneous 7–10 Hz oscillation (Wu et al. 1999) in which LFP and VSD signals are well correlated. (Modified from Jin et al. 2002)

events are two independent variables. Higher synchrony (a larger portion of neurons depolarizing in each time bin) are not always accompanied by longer duration.

Figure 7.3b-5 shows an oscillation around 10 Hz, which can be induced by bathing the slice in low Mg media (Flint and Connors 1996), or adding carbarchol

to the media (Lukatch and MacIver 1997). The oscillations are seen in both VSD and LFP recordings and the VSD and LFP signals had very similar waveforms and similar frequency compositions (Wu et al. 1999; Bao and Wu 2003).

In general, low frequency (~10 Hz) oscillations can be seen in both LFP and VSD recordings (Wu et al. 1999; Bao and Wu 2003); High frequency oscillations (~40 Hz), can be seen in LFPs but cannot be seen in VSD recordings (However, see Mann et al. 2005). The waveform of the VSD and LFP signals can be largely different.

One explanation for why waveforms of VSD and LFP can be different is that the VSD and LFP record different signals from the active neurons in the cortex. VSD signals are linearly correlated to the potential changes of all stained membranes under one detector. LFP signals, on the other hand, are a non-linear summation of the current sources distributed around the tip of the electrode and thus its amplitude decreases with the square of the distance between the source and the electrode. When an oscillation contains synchronized neuronal populations, the VSD and LFP recordings would have similar waveforms. When oscillations are organized in local ensembles and the ensembles with different phases are overlapping spatially, the VSD signal may fail to see the oscillations while LFP electrode may still pick up oscillations from neurons near the electrode. The examples below further show that VSD signal may show no oscillation in a phase singularity of spiral waves when oscillations with all phases are mixed (Fig. 7.5).

14 Examples

Over the last 30 years, many authors have published VSD imaging studies of population activities in brain slices (just to list a few, Grinvald et al. 1982a, 1982b; Albowitz and Kuhnt 1993; Colom and Saggau 1994; Tanifuji et al. 1994; Hirota et al. 1995; Tsau et al. 1998; Demir et al. 1999; Tsau et al. 1999; Wu et al. 1999; Demir et al. 2000; Laaris et al. 2000; Mochida et al. 2001; Wu et al. 2001; Huang et al. 2004; Bai et al. 2006; Hirata and Sawaguchi 2008). Below, we will show three recent examples of spatiotemporal patterns in rodent neocortex. The signals in these examples must be measured with high sensitivity and in single trials, because averaging will obscure the dynamic spatiotemporal patterns.

14.1 Spiral Waves

When rodent cortical slices were perfused with carbachol and bicuculline, oscillations around 10 Hz develop (Lukatch and MacIver 1997) and such oscillations can be reliably observed in VSD signals (Fig. 7.4b). The spatiotemporal coupling of such oscillations manifests as propagating waves; at each cycle of oscillation a
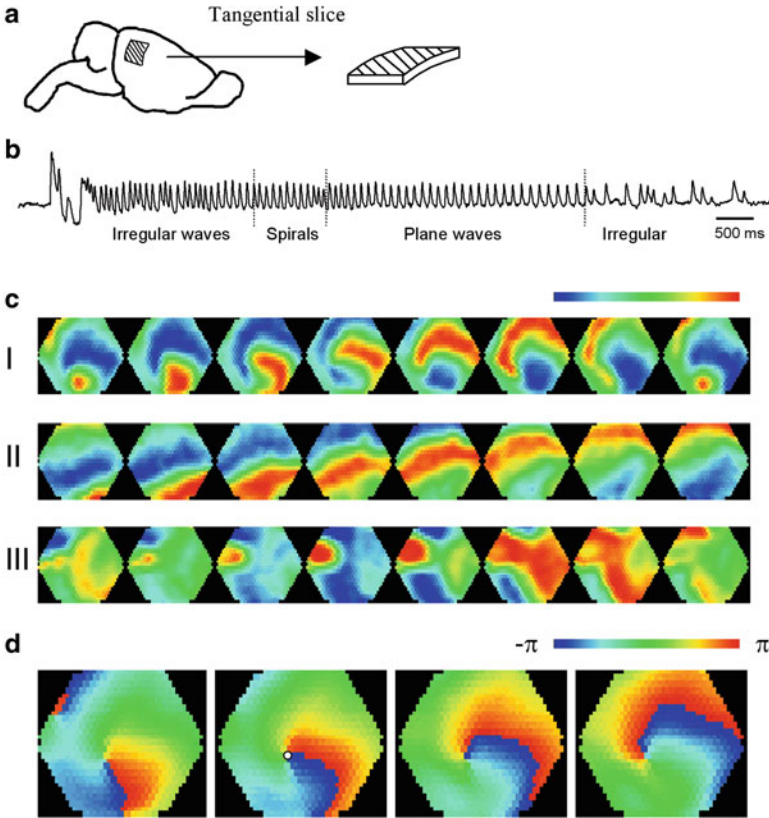
Fig. 7.4 Propagating waves in rat cortical slice. (**a**) The slice made as a 6×6-mm^2 tangential patch from rat visual cortex. (**b**) VSD signals of oscillations induced by bathing the slice in 100 μM carbachol and 10 μM bicuculline. Three types of wave patterns during one episode of oscillations (spirals, plane and irregular) can be identified from imaging data in (**c**). (**c**) Pseudo-color amplitude images during the oscillation epoch. In each row eight frames (12 ms inter-frame interval) are selected from thousands of consecutive frames take at a rate of 0.6 ms/frame. (**c-I**) Spirals, as a rotating wave around a center. (**c-II**) Plane waves, as a low curvature wave front moving across the field. (**c-III**) Irregular waves, as multiple wave fronts interacting with each other, sending waves with variety of velocities and directions. (**d**) Phase maps of a spiral wave. Color represents the oscillation phase between $-\pi$ and π according to a linear scale (*top right*). (Modified from data in Huang et al. 2004)

wave of activity propagates through the tissue (Bao and Wu 2003). When cortical slices are sectioned in a tangential plane (Fig. 7.4a), these waves are allowed to propagate in two-dimensions with a variety of patterns, such as spirals, target/ring, plane, and irregular waves (Fig. 7.4c). Plane waves have straight traveling paths across the tissue; target/ring waves develop from a center and propagate outward; Irregular waves have multiple simultaneous wave fronts with unstable directions and velocities. Spiral waves, likely arising out of the interactions of multiple plane waves, appeared as a wave front rotating around a center. Each cycle of the rotation

was associated with a cycle of the oscillation. In experiments, spiral waves were observed in 48 % of the recording trials (Huang et al. 2004). Both clockwise and counter clockwise rotations are observed during different oscillation epochs from the same slice.

In the phase map of a spiral wave, the highest spatial phase gradient is observed at the pivot of the spiral (Fig. 7.4d, white dot), which is defined as a "phase singularity". The presence of phase singularity distinguishes spiral from other types of rotating waves and is the hallmark of a true spiral wave (Ermentrout and Kleinfeld 2001; Winfree 2001; Jalife 2003). Phase singularities in cortical slices have been hypothesized as a small region containing oscillating neurons with nearly all phases represented between $-\pi$ and π (Huang et al. 2004), with the phase mixing resulting in amplitude reduction in the optical signal. In Fig. 7.5 each detector covered a circular area of 128 µm in diameter (total field of view 3.2 mm in diameter). Signals from all detectors showed high amplitude oscillations before the formation of spirals (Fig. 7.5a, trace k–o before the first broken vertical line). During spiral waves, the phase singularity drifts across the tissue slowly. The four detectors, k–n, alternately recorded reduced amplitude as the spiral center approached each detector in turn. Such amplitude reduction was localized at the spiral center, and this reduced amplitude propagated with drift of the spiral center (Fig. 7.5a traces k–n). At locations distant from the spiral center (e.g., location o in Fig. 7.5a), the amplitude remained high during all rotations of the spiral. In plane or ring waves, no localized region of oscillatory amplitude reduction was seen.

To further confirm that amplitude reduction was caused by superposition of anti-phased oscillations, we examined signals surrounding a spiral center. Figure 7.5b shows the signals from a group of detectors when a spiral center drifted over the center detector (C). As the spiral center hovered briefly (~200 ms, two rotations, marked as p above the traces in Fig. 7.5b) over the center detector, the amplitude was reduced (trace C). Simultaneously, the six surrounding detectors (1–6) did not show amplitude reduction but the oscillation phases exactly opposed each other symmetrically across the center (traces 2 and 5 are shown). These results suggest that the area with amplitude reduction was less than or equal to the size of our optical detector field of view (128 µm diameter). When we added the signals from the six surrounding detectors, the averaged waveform showed a similar amplitude reduction as the center detector (Fig. 7.5b, trace AVG). This combined signal was nearly identical to the central signal, as demonstrated by the small residual when the two signals were subtracted (Fig. 7.7b, trace AVG-C). These findings strongly support the hypothesis that amplitude reduction is not caused by inactivity of the neurons, but rather by the superimposition of multiple widely distributed phases surrounding the singularity, and that the spiral center was fully confined within an area of ~100 µm in diameter.

This example also demonstrates that high sensitivity and single trial recording are essential for studying dynamic events such as spirals. At locations near the spiral singularity, for example, the VSD signal is reduced tenfold, and requires an order of magnitude better sensitivity than if one were observing simple oscillatory events without such dynamic spatiotemporal patterns (Fig. 7.5).
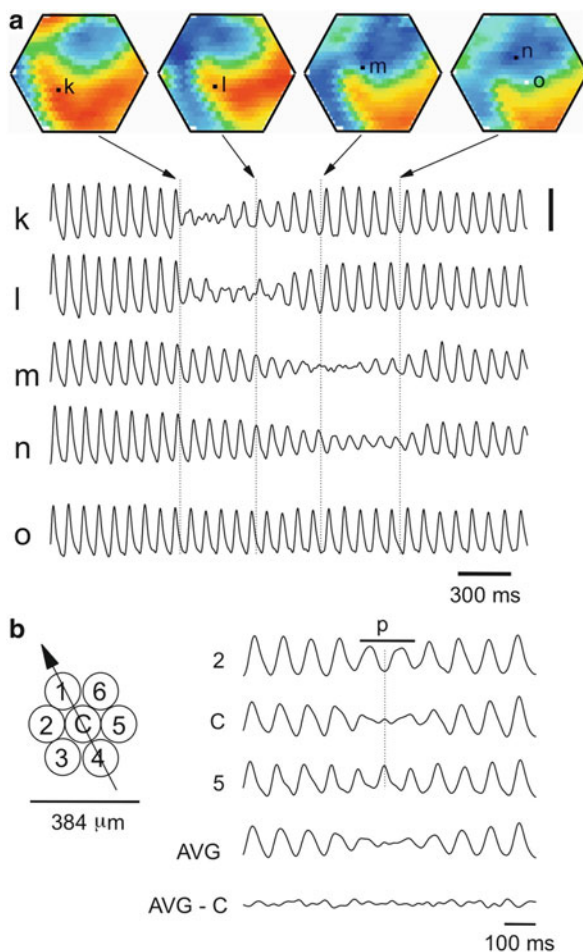
Fig. 7.5 Amplitude reduction at spiral singularity. (**a**) Color−coded representation of signal amplitude in four consecutive frames. The spirals started at about the time of the first image on the *left* and ended at the last image. Traces (k−o) Optical signals from five detectors indicated in individual frames. The *broken vertical lines* mark the times the images were taken. During spiral waves the four detectors, (k–n), sequentially recorded reduced amplitude as the spiral center approached each detector. Note that detector (o) has high amplitude signal throughout the entire period because the spiral center never reached that location. Calibration: 2×10^{-4} of rest light intensity. (**b**) *Left*: The trajectory (*arrow*) of a spiral center moving through a group of optical detectors (1–6 and C). *Right*: signals from the detectors mapped at left. *Black bar* (*p*) indicates the time when the spiral hovered over the center detector. The surrounding detectors (2, 5) did not show amplitude reduction but the oscillation phases exactly opposed each other. AVG, averaged signal of six surrounding detectors shows an amplitude reduction similar to that on the center detector C. AVG - C, numerical subtraction of trace C and AVG. These results indicate that the spiral center was fully confined within the area of the central detector. It also suggested that the amplitude reduction on trace C is caused by a superimposition of multiple phases surrounding the center detector. (Modified from Huang et al. 2004 with permission of the Society for Neuroscience)
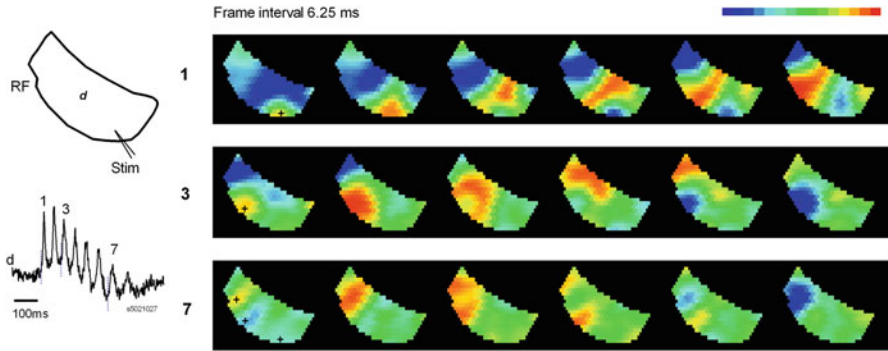
Fig. 7.6 Initiation foci of the ~25 Hz oscillation. *Left*: The orientation of the slice and stimulation sites (*top*). The VSD signal from one optical detector *d* (*bottom*). *Right*: Images of three oscillation cycles 1,3,7. Pseudo-color images generated according to a linear pseudo-color scale (*top right*, peak to *red* and valley to *blue*). All images are snapshots of 0.625 ms; the interval between images is 6.25 ms. Each row of images starts at the time marked by a *vertical broken line* in the trace display in the *left panel*. The initiation site was determined as the detector with earliest onset time and marked with *black crosses* in the first image of each row. The first spike (*1*) initiated at the location of stimulating electrode and propagated as a wave to the lateral (*top row*). Two following oscillation cycles (*3* and *7*) initiated from two different locations. All three initiation foci are marked at the first image of the *bottom row* for comparison. This optical recording trial contains 1,100 images (~0.7 s); only a few selected frames are shown for clarity. (Modified from Bai et al. 2006)

14.2   Locally Coupled Oscillations

VSD imaging has appropriate spatiotemporal resolution to reveal multiple local oscillations in brain slices. Figure 7.6 shows an evoked network oscillation (~25 Hz) in neocortical slices trigged by a single electrical shock (Bai et al. 2006). In a train of oscillations, for different cycles the waves may be initiated at different locations, suggesting local oscillators are competing for the pacemaker to initiate each oscillation cycle. The first spike initiated at the location of the stimulating electrode (Fig. 7.6, black cross in first top row image) and propagated across the slice. Two oscillation cycles, 3 and 7 initiated from two different locations (Fig. 7.6, black crosses in middle and bottom row images) and propagated in a concentric pattern surrounding their respective initiation foci. This pattern indicates that oscillations are not synchronized over space; multiple pacemakers exist and may lead different cycles alternately in turn. On the other hand, local oscillators are not completely independent, because there is a propagating wave accompanying each oscillation cycle. If the oscillators were completely independent, there would be no propagating waves. VSD imaging provides a powerful tool to study such spatial coupling of local oscillators in neocortical circuits.

14.3   High Sensitivity Optical Recordings in the Cortex In Vivo

New 'blue' dyes (e.g. RH1691), developed by Amiram Grinvald's group (Shoham et al. 1999; Chap. 2), have greatly advanced *in vivo* VSD imaging of mammalian cortex. The blue dyes are excited by red light (630 nm) that does not overlap with light absorption of hemoglobin (510–590 nm). This virtually eliminates the heart beat pulsation artifact and the signal-to-noise ratio is only limited by the movement noise and shot noise. By comparison, for the traditional 'red' dyes, such as RH795 or Di-4-ANEPPS, the pulsation artifact can sometimes exceed evoked cortical signals by an order of magnitude (Orbach et al. 1985; London et al. 1989; Shoham et al. 1999; Grinvald and Hildesheim 2004; Ma et al. 2004).

Methods for imaging mammalian cortex *in vivo* are described in detail in other chapters of this book. Some special experimental methods developed in our group have been discussed in Lippert et al. 2007. Below, we briefly demonstrate the sensitivity of *in vivo* VSD recordings.

When the cortex is properly stained, the sensitivity of VSD recording can be comparable to that of LFP recordings (Fig. 7.7). In this experiment, cortical activity was recorded with VSD imaging and LFP simultaneously from the same tissue. Comparing these two signals we found most of the peaks in the LFP showed a corresponding event in the VSD trace. Under 1.5 % isoflurane anesthesia, infrequent bursts of spontaneous activity were recorded on both electrical and optical recordings and most events within each burst correlated well between LFP and VSD signals (Fig. 7.7a). Adjusting the level of anesthesia allows us to further verify the correlation between LFP and the VSD signals. When the level of anesthesia was lowered, both VSD and LFP signals show continuous spontaneous fluctuations (Fig. 7.7b). The fluctuations in the VSD signals are unlikely to be baseline noise, since the baseline noise is much smaller in the quiescent segments of Fig. 7.7a, which were obtained from the same location in the same animal. Instead, these fluctuations are likely to be biological signals from local cortical activity, probably sleep-like oscillations or up/down states (Petersen et al. 2003a, 2003b).

LFP and VSD signals were frequently disproportionate in amplitude. In Fig. 7.7a, events labeled with dots had a higher amplitude in VSD trace while events labeled with triangles had a larger amplitude in the LFP trace. Events labeled with diamonds were seen in the LFP but not in the VSD signals. Under lower anesthesia, while the correlation between the LFP and VSD recordings decreased, many events in LFP were also seen in the VSD traces (exceptions are marked with squares in Fig. 7.7b). VSD recordings from two adjacent locations also show good correlation (bottom two traces in each panel of Fig. 7.7), further indicating that the fluctuations on the VSD traces are not noise. Since almost every event in the LFP can be recorded clearly in VSD imaging, the sensitivity of VSD measurement is comparable to that of LFP recordings. However, VSD and LFP signals have a low
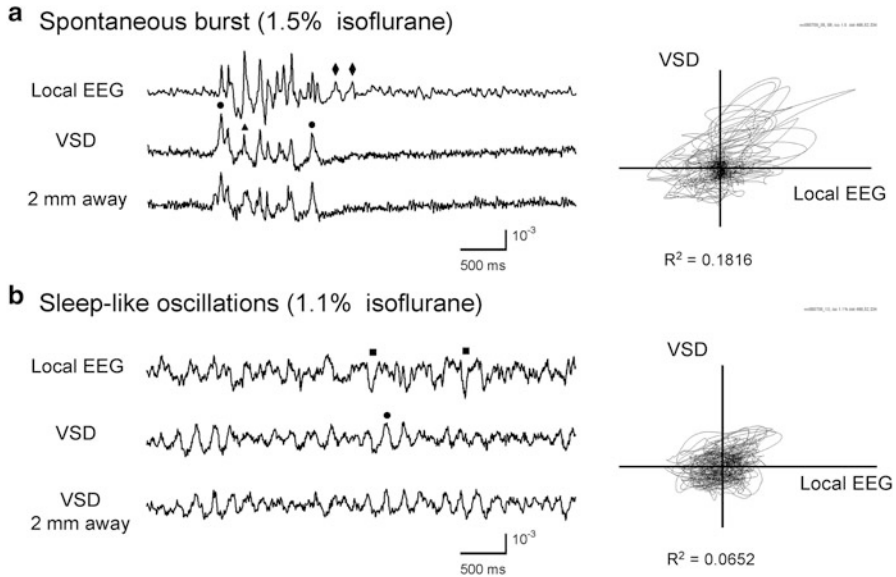
a Spontaneous burst (1.5% isoflurane)

b Sleep-like oscillations (1.1% isoflurane)

Fig. 7.7 Sensitivity of VSD recordings *in vivo*. The top two traces in each panel are LFP and VSD recordings from the same location in the visual cortex. The *bottom traces* in each panel are VSD recordings taken 2 mm away from this location. A correlation plot of the VSD and LFP of the raw data is presented on the *right*. (a) Under 1.5 % isoflurane anesthesia, the spontaneous spindle-like bursts were recorded. *Dots* mark events in which VSD has higher amplitude than LFP. *Triangles* mark events in which local field potential has higher amplitude than VSD. *Diamonds* mark events seen in local field potential but not in VSD. (b) Recordings from the same animal as in (a) about 5 min later, with isoflurane anesthesia lowered to 1.1 %. Most of the peaks in LFP are also seen in VSD, but the correlation between the two signals is lower. The baseline fluctuations cannot be attributed to noise, since recordings from the same preparation had almost no spontaneous fluctuation when anesthesia was elevated (a). (Modified from Lippert et al. 2007)

overall correlation of ~0.2 between 3 and 30 Hz (which includes 90 % of the power). This low overall correlation is probably due to some LFP peaks originating from deep cortical layers or subcortical sources.

The correlation between optical traces is much higher and each peak in the signal appears at many locations (Fig. 7.7a, b, bottom traces). The high correlation between optical traces is not due to light scattering or optical blurring between channels, because there is a small timing difference between locations, resulting in propagating waves in spatiotemporal patterns (Slovin et al. 2002; Petersen et al. 2003a, 2003b; Ferezou et al. 2006; Lippert et al. 2007; Petersen 2007; Xu et al. 2007, Mohajerani et al. 2010; Huang et al. 2010; Gao, et al. 2012). At a light intensity that results in the signal-to-noise ratio shown in Fig. 7.7, we can record up to 80–100 trials of 10 s, which is sufficient for many types of experiments. With longer recording time, the signal amplitude reduces and epileptiform spikes occasionally develop, probably due to phototoxicity.

14.4 Spatiotemporal Patters During Sleep-Like States

There are two main advantages that make high sensitivity in vivo VSD imaging unique: (1) Fast response time necessary to monitor wave dynamics which is too fast (e.g., 100 mm/ms waves) for Ca imaging. (2) High sensitivity which is mandatory for resolving patterns in single trial recordings (no averaging) to better reveal spatiotemporal characteristics of the signal. The example below demonstrates one application of the *in vivo* VSD imaging.

During sleep periods in the rat, propagating waves sweep across the cortex at a frequency of 1–4 Hz. VSD imaging provides a high spatial and temporal resolutions (464 detectors in a 5 mm diameter view field at 1,650 frames/s), sufficient for visualizing spiral routers and singularities (Huang et al. 2010). The sleep-like states were induced with slow withdrawal of pentobarbital anesthesia. The animals were first given an initial induction dose of pentobarbital (50 mg/kg), followed by tail vein infusion at a low rate of 6–9 mg/kg-h. When the initial anesthesia wore out after 2–3 h, an alternation of EEG patterns (theta/delta waves) occurred under the low maintenance infusion (Fig. 7.8a). The pentobarbital infusion rate (9–15 mg/kg-h) was then carefully adjusted for each individual animal to sustain the alternation of theta/delta wave patterns. The theta/delta alternations resemble the rapid eye movement (REM) state in rodent natural sleep (Montgomery et al., 2008). These alternations occur spontaneously, with clear difference in EEG and simultaneously recorded VSD signals (Fig. 7.8b). Spiral waves occurred frequently during both states (Examples shown in Fig. 7.8c). Double spirals with opposite rotation directions were often seen during sleep-like states (Fig. 7.8c right). The emergence of spiral waves corresponds with changes in the frequency of cortical activity. Frequency-time analysis showed that long-lasting spiral waves have prominent modulation effects on the oscillation frequencies (Fig. 7.8d). In this example frequency and power change can be clearly seen in raw trace and power spectrum, suggesting that established spiral waves have modulating effects on cortical dynamics.

Spiral waves in the intact cortex were not as stable as in slices. Most spiral waves during sleep-like states were shorter than two cycles. Ongoing background activity and long-range connections may contribute to this short duration and instability. Detailed discussion of spiral dynamics during sleep states can be found in Huang et al. 2010.
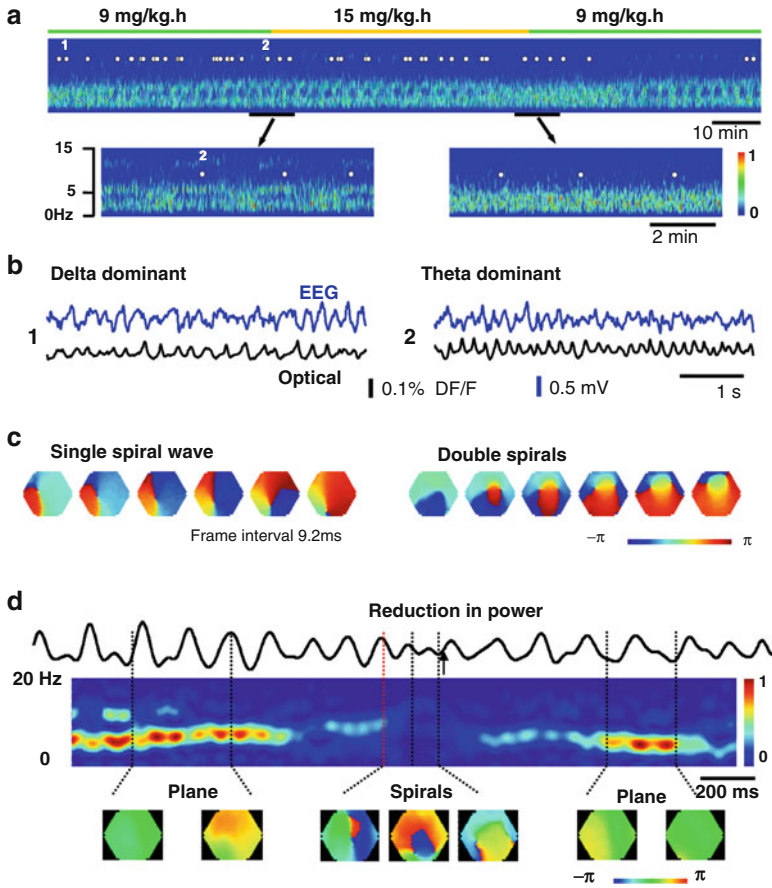
Fig. 7.8 Spatiotemporal dynamics in cortex during sleep-like states. (a) EEG is recorded by a *silver ball* electrode placed on the cortex at the corner of the imaging window. The image is the frequency-time map (frequency spectrum) made from the EEG signal. A low level of anesthesia is maintained by continuous tail vein infusion of pentobarbital at 9 mg/kg-h (*green bar*). The EEG power spectrum transitions periodically between theta (~6 Hz) and delta (1–4 Hz) dominant states when pentobarbital infusion is maintained at a low constant rate. With higher infusion rate (15 mg/kg-h) of pentobarbital (marked with *orange bar*), the alternating patterns in the EEG shifted to the delta-dominant state. *Note*: there are approximately 20 min delays of drug effects because of the slow infusion of pentobarbital. The EEG is continuously recorded and imaging trials are taken intermittently (marked by *white dots*) and two representative trials (*1, 2*) are shown in (b). Simultaneous EEG (*blue*) and optical (*black*) traces recorded during the theta-dominant ((b), *trial 2*) and delta-dominant periods ((b), *trial 1*). Spiral waves are identified from the imaging trials (c). (d) *top trace* is raw VSD signal from a representing optical detector. *Middle image* is the frequency spectrum made from the detector. Fast Fourier transform was used to analyze the power spectrum of signals in a sliding window of 300 ms. A linear pseudocolor scale is used to represent the relative power of the frequency components, *red* for high power (*1*) and blue for low power (*0*). The *Bottom images* are selected from the phase movie for identifying wave patterns. *Broken vertical lines* indicate the times for these images. The *red broken lines* mark the first cycle of spiral waves and *black arrows* mark the end of spirals (b). Ongoing cortical activity during the theta-dominant period of sleep-like state, a pair of short-lived spiral waves was identified by phase maps (*bottom images*). During spiral waves the power of the activity is significantly reduced. (Modified from Huang et al. 2010)

15 Conclusion

Cortical tissue is rich in neuropil with a relatively large area of stained excitable membrane per unit volume. During population events, cortical neurons are usually activated in ensembles; the combined dye signals from many neurons can be very large. These factors make VSD imaging a useful tool for analyzing spatiotemporal dynamics in the local circuits as well as neuronal interactions during information processing.

Imaging with VSDs provides information about when and where activation occurs and how it spreads. In cortical tissue, oscillations recorded from a LFP electrode appear as propagating waves in the VSD imaging. The wave can have complex patterns such as spirals or irregular waves and these patterns cannot be seen by recording at any one site.

Using diode arrays and an advanced vibration control, we can achieve optimum conditions for measuring population activity in brain slices and *in vivo*. With this method, about 500 locations in 1 mm^2 of cortical tissue can be monitored simultaneously with a sensitivity better than or comparable to that of LFP electrode.

References

Agmon A, Connors BW (1992) Correlation between intrinsic firing patterns and thalamocortical synaptic responses of neurons in mouse barrel cortex. J Neurosci 12:319–329

Albowitz B, Kuhnt U (1993) Evoked changes of membrane potential in guinea pig sensory neocortical slices: an analysis with voltage-sensitive dyes and a fast optical recording method. Exp Brain Res 93:213–225

Bai L, Huang X, Yang Q, Wu JY (2006) Spatiotemporal patterns of an evoked network oscillation in neocortical slices: coupled local oscillators. J Neurophysiol 96:2528–2538

Bao W, Wu JY (2003) Propagating wave and irregular dynamics: spatiotemporal patterns of cholinergic theta oscillations in neocortex in vitro. J Neurophysiol 90:333–341

Cohen LB, Salzberg BM (1978) Optical measurement of membrane potential. Rev Physiol Biochem Pharmacol 83:35–88

Cohen LB, Lesher S (1986) Optical monitoring of membrane potential: methods of multisite optical measurement. Soc Gen Physiol Ser 40:71–99

Cohen LB, Keynes RD, Hille B (1968) Light scattering and birefringence changes during nerve activity. Nature 218:438–441

Colom LV, Saggau P (1994) Spontaneous interictal-like activity originates in multiple areas of the CA2-CA3 region of hippocampal slices. J Neurophysiol 71:1574–1585

Demir R, Haberly LB, Jackson MB (1999) Sustained and accelerating activity at two discrete sites generate epileptiform discharges in slices of piriform cortex. J Neurosci 19:1294–1306

Demir R, Haberly LB, Jackson MB (2000) Characteristics of plateau activity during the latent period prior to epileptiform discharges in slices from rat piriform cortex. J Neurophysiol 83:1088–1098

Ermentrout GB, Kleinfeld D (2001) Traveling electrical waves in cortex: insights from phase dynamics and speculation on a computational role. Neuron 29:33–44

Ferezou I, Bolea S, Petersen CC (2006) Visualizing the cortical representation of whisker touch: voltage-sensitive dye imaging in freely moving mice. Neuron 50:617–629

Flint AC, Connors BW (1996) Two types of network oscillations in neocortex mediated by distinct glutamate receptor subtypes and neuronal populations. J Neurophysiol 75:951–957

Gao X, Xu W, Wang Z, Takagaki K, Li B, Wu JY (2012) Interactions between two propagating waves in rat visual cortex. Neurosci 216:57–69

Grinvald A, Hildesheim R (2004) VSDI: a new era in functional imaging of cortical dynamics. Nat Rev Neurosci 5:874–885

Grinvald A, Manker A, Segal M (1982a) Visualization of the spread of electrical activity in rat hippocampal slices by voltage-sensitive optical probes. J Physiol 333:269–291

Grinvald A, Hildesheim R, Farber IC, Anglister L (1982b) Improved fluorescent probes for the measurement of rapid changes in membrane potential. Biophys J 39:301–308

Gupta RK, Salzberg BM, Grinvald A, Cohen LB, Kamino K, Lesher S, Boyle MB, Waggoner AS, Wang CH (1981) Improvements in optical methods for measuring rapid changes in membrane potential. J Membr Biol 58:123–137

Hirata Y, Sawaguchi T (2008) Functional columns in the primate prefrontal cortex revealed by optical imaging in vitro. Neurosci Res 61:1–10

Hirota A, Sato K, Momose-Sato Y, Sakai T, Kamino K (1995) A new simultaneous 1020-site optical recording system for monitoring neural activity using voltage-sensitive dyes. J Neurosci Methods 56:187–194

Huang X, Troy WC, Yang Q, Ma H, Laing CR, Schiff SJ, Wu JY (2004) Spiral waves in disinhibited mammalian neocortex. J Neurosci 24:9897–9902

Huang X, Xu W, Liang J, Takagaki K, Gao X, Wu JY (2010) Spiral wave dynamics in neocortex. Neuron 68:978–990

Jalife J (2003) Rotors and spiral waves in atrial fibrillation. J Cardiovasc Electrophysiol 14:776–780

Jin W, Zhang RJ, Wu JY (2002) Voltage-sensitive dye imaging of population neuronal activity in cortical tissue. J Neurosci Methods 115:13–27

Kleinfeld D, Delaney KR (1996) Distributed representation of vibrissa movement in the upper layers of somatosensory cortex revealed with voltage-sensitive dyes. J Comp Neurol 375:89–108

Kojima S, Nakamura T, Nidaira T, Nakamura K, Ooashi N, Ito E, Watase K, Tanaka K, Wada K, Kudo Y, Miyakawa H (1999) Optical detection of synaptically induced glutamate transport in hippocampal slices. J Neurosci 19:2580–2588

Laaris N, Carlson GC, Keller A (2000) Thalamic-evoked synaptic interactions in barrel cortex revealed by optical imaging. J Neurosci 20:1529–1537

Lippert MT, Takagaki K, Xu W, Huang X, Wu JY (2007) Methods for voltage-sensitive dye imaging of rat cortical activity with high signal-to-noise ratio. J Neurophysiol 98:502–512

Loew LM, Cohen LB, Dix J, Fluhler EN, Montana V, Salama G, Wu JY (1992) A naphthyl analog of the aminostyryl pyridinium class of potentiometric membrane dyes shows consistent sensitivity in a variety of tissue, cell, and model membrane preparations. J Membr Biol 130:1–10

London JA, Cohen LB, Wu JY (1989) Optical recordings of the cortical response to whisker stimulation before and after the addition of an epileptogenic agent. J Neurosci 9:2182–2190

Luhmann HJ, Prince DA (1990) Transient expression of polysynaptic NMDA receptor-mediated activity during neocortical development. Neurosci Lett 111:109–115

Lukatch HS, MacIver MB (1997) Physiology, pharmacology, and topography of cholinergic neocortical oscillations in vitro. J Neurophysiol 77:2427–2445

Ma HT, Wu CH, Wu JY (2004) Initiation of spontaneous epileptiform events in the rat neocortex in vivo. J Neurophysiol 91:934–945

MacLean JN, Fenstermaker V, Watson BO, Yuste R (2006) A visual thalamocortical slice. Nat Methods 3:129–134

Mann EO, Radcliffe CA, Paulsen O (2005) Hippocampal gamma-frequency oscillations: from interneurones to pyramidal cells, and back. J Physiol 562:55–63

Metherate R, Cruikshank SJ (1999) Thalamocortical inputs trigger a propagating envelope of gamma-band activity in auditory cortex in vitro. Exp Brain Res 126:160–174

Mochida H, Sato K, Arai Y, Sasaki S, Kamino K, Momose-Sato Y (2001) Optical imaging of spreading depolarization waves triggered by spinal nerve stimulation in the chick embryo: possible mechanisms for large-scale coactivation of the central nervous system. Eur J Neurosci 14:809–820

Mohajerani MH, McVea DA, Fingas M, Murphy TH (2010) Mirrored bilateral slow-wave cortical activity within local circuits revealed by fast bihemispheric voltage-sensitive dye imaging in anesthetized and awake mice. J Neurosci 30:3745–3751

Momose-Sato Y, Sato K, Arai Y, Yazawa I, Mochida H, Kamino K (1999) Evaluation of voltage-sensitive dyes for long-term recording of neural activity in the hippocampus. J Membr Biol 172:145–157

Montgomery SM, Sirota A, Buzsaki G (2008) Theta and gamma coordination of hippocampal networks during waking and rapid eye movement sleep. J Neurosci 28:6731–6741

Orbach HS, Cohen LB, Grinvald A (1985) Optical mapping of electrical activity in rat somato-sensory and visual cortex. J Neurosci 5:1886–1895

Petersen CC (2007) The functional organization of the barrel cortex. Neuron 56:339–355

Petersen CC, Grinvald A, Sakmann B (2003a) Spatiotemporal dynamics of sensory responses in layer 2/3 of rat barrel cortex measured in vivo by voltage-sensitive dye imaging combined with whole-cell voltage recordings and neuron reconstructions. J Neurosci 23:1298–1309

Petersen CC, Hahn TT, Mehta M, Grinvald A, Sakmann B (2003b) Interaction of sensory responses with spontaneous depolarization in layer 2/3 barrel cortex. Proc Natl Acad Sci U S A 100:13638–13643

Prechtl JC, Cohen LB, Pesaran B, Mitra PP, Kleinfeld D (1997) Visual stimuli induce waves of electrical activity in turtle cortex. Proc Natl Acad Sci U S A 94:7621–7626

Ross WN, Salzberg BM, Cohen LB, Grinvald A, Davila HV, Waggoner AS, Wang CH (1977) Changes in absorption, fluorescence, dichroism, and Birefringence in stained giant axons: : optical measurement of membrane potential. J Membr Biol 33:141–183

Senseman DM, Vasquez S, Nash PL (1990) Animated pseudocolor activity maps PAMs: Scientific visualization of brain electrical activity. In: Schild D (ed) Chemosensory information processing, vol H39, NATO ASI series. Springer, Berlin, pp 329–347

Shoham D, Glaser DE, Arieli A, Kenet T, Wijnbergen C, Toledo Y, Hildesheim R, Grinvald A (1999) Imaging cortical dynamics at high spatial and temporal resolution with novel blue voltage-sensitive dyes. Neuron 24:791–802

Slovin H, Arieli A, Hildesheim R, Grinvald A (2002) Long-term voltage-sensitive dye imaging reveals cortical dynamics in behaving monkeys. J Neurophysiol 88:3421–3438

Tanifuji M, Sugiyama T, Murase K (1994) Horizontal propagation of excitation in rat visual cortical slices revealed by optical imaging. Science 266:1057–1059

Tasaki I, Watanabe A, Sandlin R, Carnay L (1968) Changes in fluorescence, turbidity, and birefringence associated with nerve excitation. Proc Natl Acad Sci U S A 61:883–888

Tsau Y, Guan L, Wu JY (1998) Initiation of spontaneous epileptiform activity in the neocortical slice. J Neurophysiol 80:978–982

Tsau Y, Guan L, Wu JY (1999) Epileptiform activity can be initiated in various neocortical layers: an optical imaging study. J Neurophysiol 82:1965–1973

Winfree AT (2001) The geometry of biological time. Springer, New York, NY

Wu JY, Cohen LB (1993) Fast multisite optical measurement of membrane potential. In: Mason WT (ed) Biological techniques: fluorescent and luminescent probes for biological activity. Academic, New York, NY, pp 389–404

Wu JY, Guan L, Tsau Y (1999) Propagating activation during oscillations and evoked responses in neocortical slices. J Neurosci 19:5005–5015

Wu JY, Guan L, Bai L, Yang Q (2001) Spatiotemporal properties of an evoked population activity in rat sensory cortical slices. J Neurophysiol 86:2461–2474

Xu W, Huang X, Takagaki K, Wu JY (2007) Compression and reflection of visually evoked cortical waves. Neuron 55:119–129

Zecevic D (1996) Multiple spike-initiation zones in single neurons revealed by voltage-sensitive dyes. Nature 381:322–325